CHEMISTRY
A EUROPEAN JOURNAL

DOI: 10.1002/chem.200901421

Selective Metal-Cation Recognition by [2.2]Ferrocenophanes: The Cases of Zinc- and Lithium-Sensing

Francisco Otón,[a, b] Imma Ratera,[b] Arturo Espinosa,[a] Klaus Wurtz,[c] Teodor Parella,[d] Alberto Tárraga,*[a] Jaume Veciana,*[b] and Pedro Molina*[a]

Abstract: The synthesis, electrochemical, optical, and cation-sensing properties of [2.2]ferrocenophanes, in which the two ferrocene subunits are linked through two aldiminic or iminophosphorane moieties, are reported. The new compounds show remarkably selective cation-sensing properties due to the presence of redox-active units (ferrocene) and aza-unsaturated functionalities that are able to act as putative cation-binding sites. In this structural motif, the aldimine groups act as a highly selective binding site for Zn^{2+} cations, whereas the iminophosphorane bridges display an unusually strong binding affinity towards Li^{+} cations, which could be explained by an additional Li···Fe interaction. The X-ray structure of the complex **4**·Li^{+} as well as detailed NMR spectroscopic studies, both in solution and in the solid state, support this assessment. Experimental data and conclusions about the cation-sensing capabilities of this family of compounds are supported by DFT calculations.

Keywords: chemosensors · cyclophanes · imines · iron · lithium · zinc

Introduction

The design and development of small molecules for sensing applications is currently of great interest in supramolecular chemistry.[1] Research activities in this area are mainly focused on the design and synthesis of molecules that can lead to practical chemosensors. To make a useful chemosensor molecule, the compound must contain a "signaling site", such as a chromophore, fluorophore, or redox-active center, along with a "binding site" that meets several electronic and structural requirements that are rather strict for the selective recognition of some elusive metal ions, for example, the Li^{+} and Zn^{2+} cations. In this context, substituted ferrocene has largely proved to be a simple and remarkably robust building block for the preparation of these derivatives, which have been considered as prototype chemosensor molecules owing to their interesting electrochemical and optical sensing properties.[2] In this context, multinuclear [*m.n*]ferrocenophanes linked by all-carbon π bridges with a well-defined topology have received considerable attention.[3] The ferrocenophanic architectures that additionally incorporate sites in the bridges that would allow the binding of metal ions would provide potential applications for this structural motif. Especially attractive from this point of view are the almost unexplored [*m.n*]ferrocenophanes bearing nitrogen-containing bridges, with only the preparation and sensing properties of two multinuclear nitrogen-rich [4.4]- and [3.3]ferrocenophanes having recently been reported.[4]

On the other hand, there are a few precedents for iron—metal-ion interactions in several complexes of transition-metal ions in which a ferrocenyl group acts as a donor in the coordination sphere of the metal ion.[5] In this context, it has been reported that ferrocene behaves as a moderately strong base towards the Li^{+} cation to form complexes.[6] The

[a] Dr. F. Otón, Dr. A. Espinosa, Prof. A. Tárraga, Prof. P. Molina
Universidad de Murcia, Departamento de Química Orgánica
Facultad de Química
Campus de Espinardo, 30100 Murcia (Spain)
Fax: (+34) 968-364149
E-mail: pmolina@um.es
atarraga@um.es

[b] Dr. F. Otón, Dr. I. Ratera, Prof. J. Veciana
Institut de Ciencia de Materials de Barcelona (CSIC)/CIBER-BBN
Campus Universitari de Bellaterra, 08193 Cerdanyola (Spain)
Fax: (+34) 935805729
E-mail: vecianaj@icmab.es

[c] Dr. K. Wurtz
Institut für Allgemeine Anorganische und Theoretische Chemie
Universität Innsbruck
Innrain 52a, 6020 Innsbruck (Austria)

[d] Dr. T. Parella
Servei RMN, Universitat Autònoma de Barcelona
Campus Universitari de Bellaterra, 08193 Cerdanyola (Spain)

Supporting information for this article is available on the WWW under http://dx.doi.org/10.1002/chem.200901421.

interaction of ferrocene with Li^+ has previously been studied theoretically by Ugalde and co-workers,[6b] who located two minima on the energy surface. The most stable isomer of this complex has Li^+ above one of the cyclopentadienyl rings, whereas in the less stable isomer, the Li^+ binds directly to the central iron metal. This latter isomer has been characterized as a planetary system in the sense that Li^+ has one thermally accessible planar orbit around the central ferrocene moiety. Later, Scheibitz et al.[7] provided experimental evidence for the existence of the latter structure. However, the presence of charged bridges in the ferrocenophane would strongly favor lithium coordination and the binding effect of ferrocene would be blurred. Owing to the fact that Li^+ placement in this type of structure is directed by the charged moieties, a planetary system in a ferrocene–Li^+ complex without an anionic bridge would be of special interest.

Another interesting metal ion to investigate is Zn^{2+} because this metal is the second most abundant transition metal following iron and a fundamental element in biological systems.[8] Zinc is an essential nutrient required for normal growth and development[9] and for key cellular processes such as DNA repair[10] and apoptosis.[11] Currently there is a high demand for systems able to sense the Zn^{2+} cation, which is spectroscopically silent because of its $3d^{10}4s^0$ electronic configuration. Moreover, the development of simple chemosensors that can discriminate Zn^{2+} from Cd^{2+} is still a challenge because cadmium and zinc are in the same group of the periodic table and have similar properties, usually causing similar spectral changes after interactions with chemosensors.[12]

In this paper we describe the preparation of multinuclear [2.2]ferrocenophanes linked by aza-unsaturated chains, namely aldiminic or iminophosphorane functionalities. In addition to the well-known ability of the aldiminic group to act as a binding site for metal cations, the iminophosphorane R_3PNR (nitrogen analogues of phosphorus ylides) functionality has been proven to coordinate transition metals through the approximately sp^2-hybridized nitrogen atom to give stable complexes.[13] The combined effects of the binding capability of the bridges and the close proximity between the redox units makes this new rigid structural motif a likely candidate for displaying selective cation-sensing properties. Moreover, the close proximity between the redox centers and the binding sites could allow these ferrocene derivatives to be used to monitor the binding of metal cations and also to behave as actuators through the progressive electrochemical release of the metal cation with the consequent decrease in the binding constant upon electrochemical oxidation. Furthermore, we also report on the first isolation of a ferrocene–lithium complex, based on a multinuclear [2.2]ferrocenophane linked by iminophosphorane functionalities, that provides experimental evidence of the planar orbit around the central ferrocene moiety. Additionally, we also describe a bis-imino[2.2]ferrocenophane that selectively binds Zn^{2+} in the presence of Cd^{2+} cations.

Results and Discussion

Synthesis and conformational analysis: Preparation of the target [2.2]metallocenophanes was achieved starting from either 1,1′-diazidoferrocene (**1**) or the bis(iminophosphorane) 1,1′-bis(*N*-triphenylphosphoranylideneamino)ferrocene (**2**), readily available by Staudinger reaction of **1** with triphenylphosphine.[14] Bis(iminophosphorane) **2** displays the typical reactivity shown by monoiminophosphoranes in aza-Wittig type reactions towards carbonyl compounds.[15] Thus, aza-Wittig reaction with equimolecular amounts of 1,1′-diformylferrocene provided the bis(aldimine)ferrocene **3** in a yield of 72% (Scheme 1). Compound **4** bearing two aza-phospha bridges was prepared in a yield of 73% by Staudinger reaction of 1,1′-diazidoferrocene (**1**) and 1,1′-bis(diphenylphosphino)ferrocene at room temperature in CH_2Cl_2 under high dilution conditions.

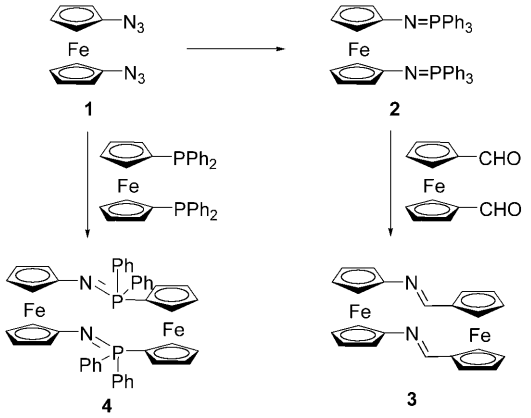

Scheme 1. Preparation of the new ferrocene receptors **3** and **4.**

The structures of both [2.2]metallocenophanes were determined by standard spectroscopic techniques (IR, ^1H NMR, and ^{13}C NMR spectroscopy), mass spectrometry, and elemental analyses. All data were in agreement with the proposed structures.

The presence of two different ferrocene moieties in the [2.2]ferrocenophane **3** is clearly revealed by analysis of its ^1H NMR spectrum. Thus, whereas a singlet at $\delta = 9.39$ ppm is observed for the iminic protons within the asymmetric imine bridges, four different signals arising from the ferrocenyl units ($H_\alpha = 4.07$, $H_{\alpha'} = 4.24$, $H_\beta = 5.12$, and $H_{\beta'} = 5.44$ ppm) are observed, which are associated with the two different monosubstituted cyclopentadienyl (Cp) rings belonging to the two ferrocene subunits. Additionally, a temperature-dependent ^1H NMR experiment was carried out to study the conformational behavior of ligand **3** in solution (Figure 1). At 268 K, a peak broadening is clearly observed and at 211 K a new pattern of peaks is noticed: All the signals appearing at room temperature are now split into two, the coalescence temperature being 248 K. This demonstrates

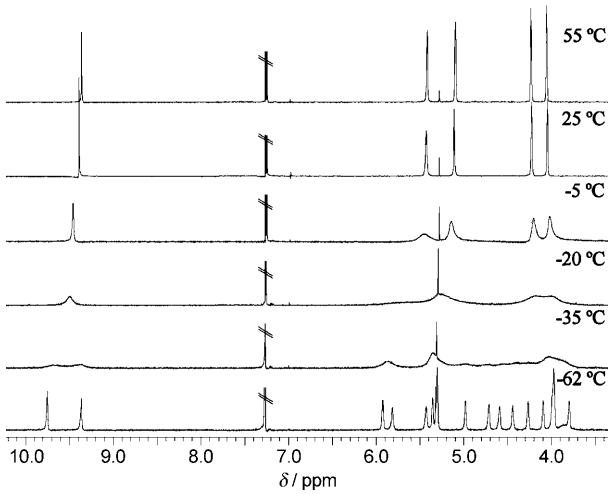

Figure 1. Evolution of the ^{1}H NMR spectrum of the receptor **3** ($c = 5 \times 10^{-3}$ M, $CDCl_3$) with temperature, revealing the conformational interchange in solution.

the presence in solution of two different conformers that are very similar in energy.

DFT quantum chemical calculations were performed to provide the required structural and thermodynamic information to understand these conformational equilibria. Indeed, two minima close in energy were located on the potential energy surface of compound **3**. The absolute minimum has C_s symmetry (**3**^{Cs}) with both imine nitrogen atoms pointing to the same side of the molecule (Figure 2). By rotation around the outer linkages of one of the imine bridges, the structure of the other C_2-symmetric diastereomer (**3**^{C2}) can be reached through a rather low energy barrier, corresponding to the transition estate **3**^{TS}, which accounts for the relatively high coalescence temperature ($T = 248$ K) found for **3**. In addition, the low difference in energy calculated between the two species would explain why they are present in comparable amounts in equilibrium (e.g., 59.4:40.6 in the gas-phase).

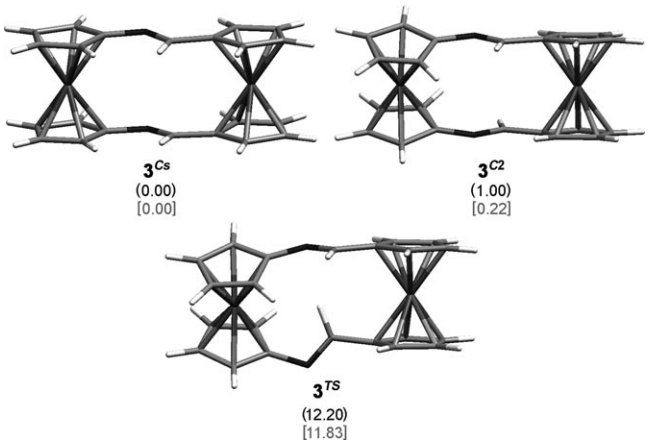

Figure 2. Calculated structures of the two conformational minima of compound **3** and the transition state (TS) for interconversion between the two minima. The calculated relative Gibbs free energies (kcal mol^{-1}) are given in brackets in $CHCl_3$ solution (black) and in the gas-phase (grey).

Receptor **4** exhibits in $CDCl_3$ solution a broad and poorly defined ^{1}H NMR spectrum, probably due to a slow interconversion of the conformers. The ferrocene protons appear as six multiplets at $\delta = 3.62$, 3.68, 3.82, 4.15, 4.21, and 4.43 ppm in a ratio of 4:6:2:1:2:1 and the aromatic protons as two broad multiplets at $\delta = 7.49$ and 7.54 ppm. A temperature-dependent ^{1}H NMR study was also carried out. However, significant changes in the ^{1}H NMR spectrum were not observed, which suggests a more rigid conformational space than for the [2.2]ferrocenophane **3**.

DFT calculations were also performed on compound **4**. A thorough inspection of the potential energy surface of this compound reveals that the absolute C_2-symmetric minimum **4**^{C2} (Figure 3) is located in a flat well surrounded by at least

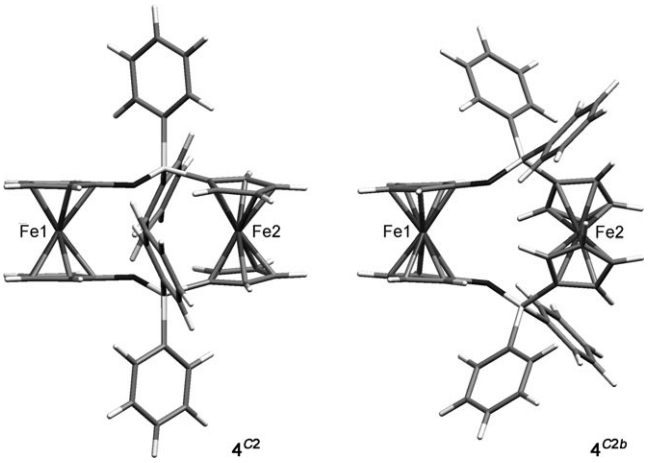

Figure 3. Calculated structures of the C_2-symmetric minima **4**^{C2} (left) and **4**^{C2b} (right).

two other easily interchangeable local minima with broken symmetries (**4**^{ns}) that are only 0.27 kcal mol^{-1} less stable. Ferrocenophane **4**^{C2} features two axial and two equatorial phenyl groups (almost linear and orthogonal $\phi_{P\cdots P-Ph}$ angles, respectively; Table 1) that can interchange via another C_2-symmetric local minimum **4**^{C2b} with *P*-phenyl substituents that are half-axial/half-equatorial in character and destabilized by only 1.92 kcal mol^{-1}. The absolute minimum **4**^{C2} displays a rather elongated geometry with a relatively large Fe···Fe distance ($d_{Fe\cdots Fe} = 6.360$ Å) and a short distance between the bridges ($d_{N\cdots N} = 3.278$ Å) with almost parallel ferrocenes (small $\theta_{Cp1\#-Fe1\cdots Fe2-Cp2\#}$ dihedral; $Cp_i^{\#}$ represents the centroid of ring Cp_i; Table 1). Two hydrogen bonds between

Table 1. Important geometric parameters for the structure calculated for ligand **4** and its calculated and experimental Li^+ complexes.

	4^{C2}	**4**^{C2b}	**4**^{C2}·Li^+	**4**^{ns2}·Li^+	**4**·$Li^+(C_6H_5)_4B^-$
$d_{Fe1\cdots Fe2}$ [Å]	6.360	5.628	5.737	6.206	6.277
$d_{N\cdots N}$ [Å]	3.278	4.391	3.786	3.430	2.853
$d_{P\cdots P}$ [Å]	4.734	5.465	5.553	5.156	4.705
$\phi_{P\cdots P-Ph}$ [°]	164.1	132.1	132.1	167.2, 143.9	152.3, 150.7
	92.7	119.7	120.3	87.7, 110.6	98.0, 99.0
$\theta_{Cp1\#-Fe1\cdots Fe2-Cp2\#}$ [°]	10.2	46.4	56.4	17.4, 17.9	2.3, 1.4

each nitrogen atom and a Cp–H atom and an *ortho*-hydrogen atom of the equatorial phenyl group ($d_{N\cdots H}=2.828$ and 2.348 Å, respectively) partially fixes the most stable conformation. This would explain the relatively slow interconversion between two identical $\mathbf{4}^{C2}$ conformers on the NMR timescale and accounts for the observed signal-broadening (see above). Very significantly (see below), the second local minimum $\mathbf{4}^{C2b}$ is less stretched with a shorter intermetallic distance ($d_{Fe\cdots Fe}=5.628$ Å) and a larger distance between the ferrocenyl connecting bridges ($d_{N\cdots N}=4.391$ Å) caused by a rotation in the relative orientation of the two ferrocenes (Table 1).

The structures calculated for the [2.2]ferrocenophanes **3** and **4**, in which the two nitrogen-based donor groups are close and point to the same side of the molecule, suggest that these compounds could be useful for the molecular recognition of metal-cation species.

Metal-ion-sensing properties: Receptors **3** and **4** present, as special features, a particularly rigid backbone and two nitrogen donor atoms appropriately arranged with respect to the ferrocenyl units, conferring on them very interesting complexation properties. Another interesting attribute of the new ferrocenophanes reported herein is the presence of two metal-ion binding sites on the bridges which are in proximity to a ferrocene redox-active moiety. Consequently, the behavior of receptors **3** and **4** towards complexation with several metal cations has been studied by electrochemical methods, UV/Vis spectroscopy, and NMR spectroscopy. To gain an insight into the binding properties of the two ligands, a set of alkali-metal ions (Li^+, Na^+, and K^+), alkaline-earth-metal ions (Mg^{2+} and Ca^{2+}), and transition-metal ions (Ni^{2+}, Cu^{2+}, Zn^{2+}, Cd^{2+}, and Hg^{2+}), as their triflate or perchlorate salts, were tested.

Receptor 3: To explore the electrochemical sensing behavior of receptor **3** cyclic voltammetry (CV) and differential pulse voltammetry (DPV) were carried out at room temperature. The CV response in CH_2Cl_2/CH_3CN (4:1) containing 0.1 M $[n\mathrm{Bu}_4\mathrm{N}]PF_6$ as the supporting electrolyte shows two electrochemically reversible one-electron waves at $E_{1/2}=-0.06$ and 0.46 V versus the ferrocenium/ferrocene (Fc^+/Fc) redox couple corresponding to the redox processes of the two ferrocene moieties (see the Supporting Information). Similarly, DPV also exhibits two oxidation peaks at the same potentials versus Fc^+/Fc. The electrochemical changes upon addition of the above-mentioned set of metal cations to the receptor **3** was also investigated by using DPV to explore the metal recognition process more accurately.[16] Indeed, the study indicates that this receptor behaves as a selective electrochemical sensor for Zn^{2+} in CH_2Cl_2/CH_3CN (4:1). The addition of increasing amounts of Zn^{2+} to the electrochemical solution (up to 2.25 equiv) of receptor **3** caused the partial disappearance of the wave at −0.06 V and the simultaneous appearance of a new wave at 0.02 V. However, the second wave of the free receptor, at $E_{1/2}=0.46$ V, does not suffer any perceptible change during the titration. This suggests that the initially formed complex is disrupted after the first monoelectronic oxidation and, as a consequence, the second oxidation takes place on the uncomplexed mono-oxidized species $\mathbf{3}^{\cdot+}$. In other words, these results show that the $\mathbf{3}\cdot Zn^{2+}$ adduct undergoes a reversible electrochemically induced decomplexation/complexation process on a timescale faster than that of the electrochemical experiments,[17] which were carried out at 100 mV s^{-1} (see the Supporting Information). Receptor **3** underwent oxidation in the presence of Cu^{2+} and Hg^{2+} cations, whereas the addition of Li^+, Na^+, K^+, Mg^{2+}, Ca^{2+}, Cd^{2+}, and Ni^{2+} did not promote any significant change in the corresponding electrochemical responses of receptor **3**.

The metal recognition properties of the aza-bridged metallocene dyad **3** were also evaluated by UV/Vis spectroscopy. Previous studies on ferrocene-based ligands have shown that bands in the absorption spectra ascribed to the lowest-energy metal–ligand transitions are perturbed upon metal-ion complexation.[18] Titration experiments in CH_2Cl_2/CH_3CN (4:1) solutions of receptor **3** ($c=1\times10^{-4}$ M) with the corresponding ions were performed and analyzed quantitatively.[19] No changes were observed in the UV/Vis spectra upon addition of Li^+, Na^+, K^+, Mg^{2+}, Ca^{2+}, Cd^{2+}, and Ni^{2+}, even in a large excess. However, significant modifications were observed upon addition of Cu^{2+}, Hg^{2+}, and Zn^{2+}. Thus, the addition of increasing amounts of Zn^{2+} to a solution of **3** caused the disappearance of the low-energy (LE) metal-to-ligand transition band (MLCT) at $\lambda=491$ nm ($\varepsilon=660\,\mathrm{M^{-1}cm^{-1}}$) and the progressive appearance of a new band located at $\lambda=600$ nm ($\varepsilon=1200\,\mathrm{M^{-1}cm^{-1}}$). The consequent appearance of a well-defined isosbestic point at 505 nm indicates that a neat interconversion between the uncomplexed and complexed species occurs. The shift of the LE band by 139 nm indicates that the complexation of zinc is responsible for the change in color from red to deep-green, which can be detected by the "naked eye" (Figure 4). Binding assays using the method of continuous variation (Job plot) are consistent with the formation of a complex with a 2:1 receptor/Zn^{2+} stoichiometry (see the Supporting Information). The calculated association constant and detection limit obtained from such a titration experiment.[20] are $7.9\times10^5\,\mathrm{M^{-2}}$ (error $<15\%$) and 5.7×10^{-6} M, respectively. On the other hand, addition of either Cu^{2+} or Hg^{2+} cations led to chemical oxidation of the ligand and the resulting absorption spectra were the same and identical to those obtained under electrochemical oxidation conditions.

To gain first-hand information about the mechanism of the complexation of **3** with Zn^{2+}, ^{1}H NMR experiments were also performed. Thus, addition of 1 equiv of Zn^{II} triflate in CD_3CN to a solution of receptor **3** in CD_2Cl_2/CD_3CN (4:1) gives rise to significant downfield shifts of the aldiminic protons of the bridge (from $\delta=9.32$ to 10.04 ppm, $\Delta\delta=0.72$ ppm), which confirms the direct participation of the nitrogen atoms of the imine functions in the coordination event, as initially expected. Similarly, the α and β protons of the ferrocene moieties are also shifted downfield, although to a lesser degree (from $\delta=5.21$, 4.89, 4.03, and

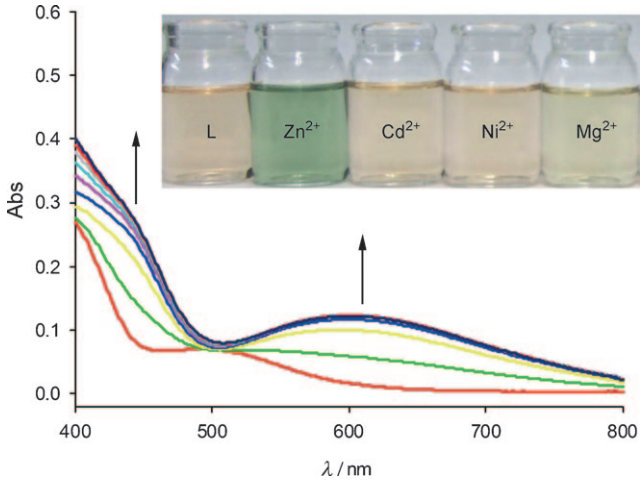

Figure 4. Variation of the visible spectrum of **3** ($c=1\times10^{-4}$ M) in CH_2Cl_2/CH_3CN (4:1) upon addition of increasing amounts of Zn^{2+}. Inset: Color change upon addition of different cations to receptor **3**.

3.81 ppm to 5.90, 5.57, 4.63, and 4.22 ppm, respectively; Figure 5).

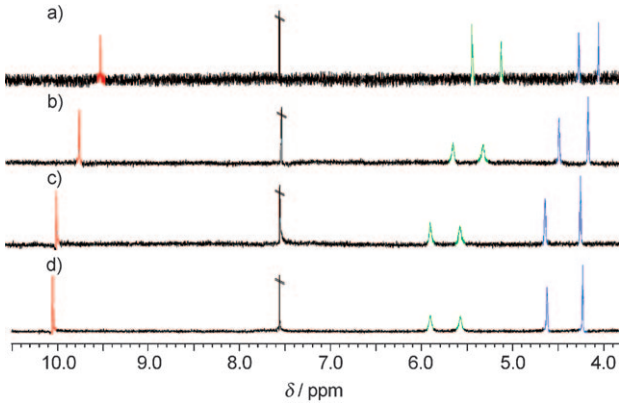

Figure 5. Evolution of the ^{1}H NMR spectra of **3** ($c=5\times10^{-3}$ M) in CD_2Cl_2/CD_3CN (4:1) solution upon addition of a) 0, b) 0.4, c) 1, and d) 2 equiv of Zn^{2+} (as the triflate salt).

*Receptor **4***: The coordination capability of receptor **4** was also studied by UV/Vis spectroscopy, electrochemical methods, and NMR spectroscopy. First, we investigated the cation coordination ability by UV/Vis spectroscopy. The spectrum of this ligand exhibits two low-energy charge transfer bands at $\lambda=480$ ($\varepsilon=1240\,M^{-1}cm^{-1}$) and 669 nm ($\varepsilon=170\,M^{-1}cm^{-1}$) and upon stepwise addition of Li^+ (from 0 to 1.1 equiv) the band at $\lambda=480$ nm suffers an important decrease in the molar absorptivity coefficient ($\varepsilon=925\,M^{-1}cm^{-1}$), whereas the band at $\lambda=669$ nm shows an increase in intensity ($\varepsilon=235\,M^{-1}cm^{-1}$). The presence of a well-defined isosbestic point at $\lambda=614$ nm demonstrates the participation of only two species in the complexation process (Figure 6). In contrast, the addition of an excess of Na^+, K^+, Ca^{2+}, or Mg^{2+} did not cause any variation in the UV/Vis spectrum of **4**, which is indicative of the lack of affinity of

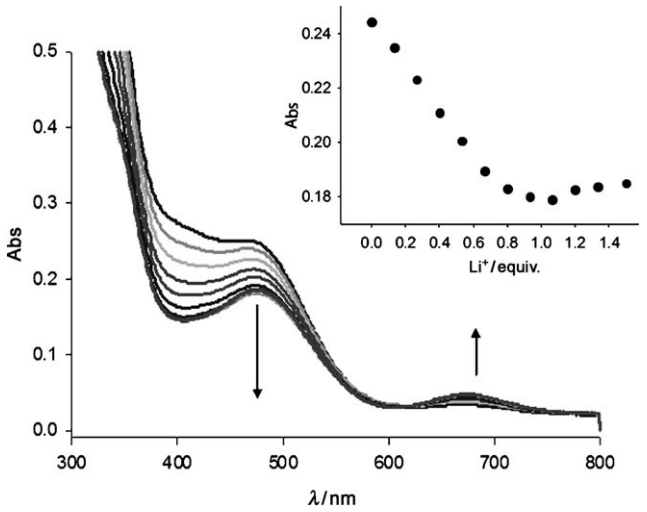

Figure 6. Variation of the UV/Vis spectrum of **4** ($c=2\times10^{-4}$ M) in THF solution upon addition of increasing amounts of Li^+ (as the perchlorate salt). Inset: Binding profile of the titration process following the band at $\lambda=480$ nm.

this receptor for larger mono- and dicationic cations. The small cavity formed by the receptor **4** probably promotes the exceptional selective binding of the small Li^+ cation over the other cations tested. From the titration data the stoichiometry of the complex was found to fit a 1:1 binding model, with $K_a>10^6\,M^{-1}$ and a detection limit of 2.3×10^{-5} M (error $<15\%$).

The electrochemical studies confirmed the results derived from the spectroscopic study. Indeed, the cyclic voltammogram (CV) of receptor **4** exhibits two electrochemically reversible waves at $E_{1/2}=-0.80$ and 0.45 V versus Fc^+/Fc (CH_2Cl_2, $c=1\times10^{-3}$ M, $[(nBu)_4N]PF_6$ as the supporting electrolyte). The first oxidation wave was assigned (Figure 7) to the oxidation of the ferrocene unit directly linked to the nitrogen atoms, whereas the second wave to the oxidation of the ferrocene linked to the phosphorus atoms.

Stepwise addition of Li^+, Na^+, K^+, Ca^{2+}, or Mg^{2+} metal cations to an electrochemical solution of receptor **4** showed that only the Li^+ metal cation (1 equiv) induces a remarkable perturbation in the electrochemical responses of the receptor, the other metal ions tested not causing any change in the electrochemical response. Thus, when Li^+ was added, the first oxidation wave dramatically shifted from $E_{1/2}=-0.80$ V to $E_{1/2}=0.03$ V ($\Delta E_{1/2}=830$ mV), whereas the potential of the second wave remained unchanged (see the Supporting Information). Such electrochemical changes can be interpreted in the same way as for compound **3** (Figure 7). Thus, upon complexation, the oxidation peak of the free ligand (red line, peak *a*) disappears and a wave is observed anodically shifted (blue line, peak *c*). However, the reduction peak of the complex **4**·Li^+ (blue line, peak *d*) appears at the same potential as that observed for the free receptor (red line, peak *b*), which indicates the absence of the Li^+ cation. A plausible explanation for this behavior is that upon oxidation of the first ferrocene unit the complex **4**·Li^+

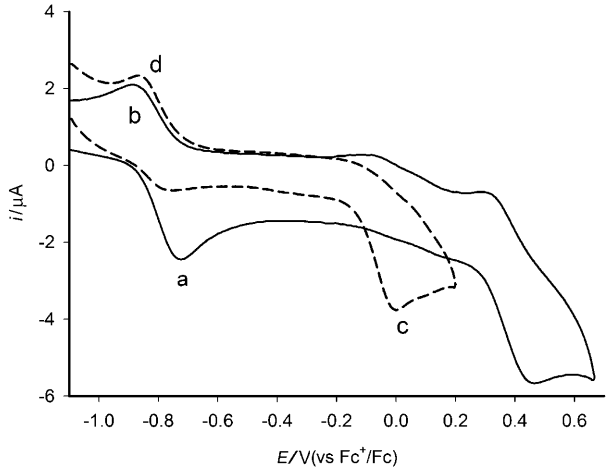

Figure 7. Cyclic voltammograms of compound **4** ($c=1\times10^{-3}$ M; solid line) in anhydrous THF solution using 0.1 M $[(n\text{Bu})_4\text{N}]\text{PF}_6$ as the supporting electrolyte at a scan rate = 0.1 V s^{-1} and the complex **4**·Li^+ (dashed line). Letters a and b correspond to peaks of the free receptor **4** and c and d to the complex **4**·Li^+.

is disrupted and the complexed Li^+ ion is expelled from the ferrocenophane and the second oxidation process takes place on the cation radical $\mathbf{4}^{\cdot+}$. In line with such electrochemical observations, the natural orbital analysis of $\mathbf{4}^{C2}$ reveals that the uppermost occupied atomic orbital (AO) is located on the Fe1 atom closest to the nitrogen substituents (−0.117 hartree) and is therefore much more readily accessible on oxidation than the highest energy 3d AO on Fe2 (−0.176 hartree), which explains the observed sequence in voltammetry for both anodic waves (see Figure 7). On the other hand, lithium complexation is expected to considerably increase the first oxidation potential (the computed energy for the uppermost 3d AOs on Fe1 and Fe2 drop to −0.224 and −0.284 hartree, respectively) in agreement with electrochemical studies (Figure 7).

The redox decomplexation process of **4**·Li^+ was confirmed by a spectroelectrochemical study. Thus, 1 equiv of Li^+ ion was added to a solution of receptor **4** to obtain the complexed ferrocenophane **4**·Li^+ species. The resulting complex was then electrochemically oxidized at 0.8 V, versus Fc^+/Fc, until complete oxidation occurred. The optical spectrum of the resulting solution was the same as that obtained by the dielectronic oxidation of the free receptor **4** to $\mathbf{4}^{2+}$, which suggests that decomplexation of the Li^+ ion occurs during the electrochemical oxidation (see the Supporting Information).

The complexation process of receptor **4** with Li^+ cations was also assessed by using ^{1}H, ^{13}C, ^{31}P, and ^{7}Li NMR spectroscopy, both in solution and in the solid state. Important changes were found upon complexation by all techniques, which is clear experimental proof for the existence of a planetary system for ferrocene–Li^+ complexes without negative charges on the bridge. Receptor **4** exhibits in CDCl_3 solution ($c=5\times10^{-3}$ M) at 25 °C a broad and poorly defined ^{1}H NMR spectrum (Figure 8a), which probably is a result of a slow interconversion of conformers, as was seen before. However, after the addition of the Li^+ cation (1 equiv), a well-defined spectrum is obtained that exhibits four multiplets in a 4:4:4:4 ratio that correspond to the ferrocene protons. Similarly, the ^{13}C NMR spectrum shows important changes upon complexation: The four doublets corresponding to the methine carbon atoms of the ferrocene moiety connected to the phosphorus atoms [$\delta=74.4$ (d, $^3J_{\text{C–P}}=10.5$ Hz), 73.9 (d, $^3J_{\text{C–P}}=10.5$ Hz), 73.4 (d, $^2J_{\text{C–P}}=12.0$ Hz), 73.3 ppm (d, $^2J_{\text{C–P}}=12.0$ Hz)] are converted into two-shifted doublets [$\delta=75.0$ (d, $^2J_{\text{C–P}}=13.4$ Hz), 74.8 ppm (d, $^3J_{\text{C–P}}=10.9$ Hz)] upon complexation. Likewise, the two singlets corresponding to the methine carbon atoms of the ferrocene group connected to the aldiminic carbon atoms of the bridge are shifted downfield from $\delta=64.2$ and 63.3 ppm to $\delta=69.02$ and 66.99 ppm, respectively. Remarkably, the quaternary *ipso*-carbon atoms of the aromatic rings are shifted by $\Delta\delta=-7.3$ ppm from 133.8 ppm (d, $^1J_{\text{C–P}}=106.4$ Hz) to 126.5 ppm (d, $^1J_{\text{C–P}}=103.4$ Hz); the methine *ortho*-, *meta*-, and *para*-carbon atoms are also shifted although to a lesser extent. A similar variation was found in the ^{7}Li NMR spectrum upon addition of receptor **4** to a solution of Li^+ salt, with a shift of $\Delta\delta=0.15$ ppm (from $\delta=3.13$ to 3.28 ppm; Figure 8b). The ^{31}P NMR spectrum of receptor **4** at 25 °C displays one signal at $\delta=27.1$ ppm, which is shifted downfield to $\delta=30.2$ ppm ($\Delta\delta=3.1$ ppm) after complex forma-

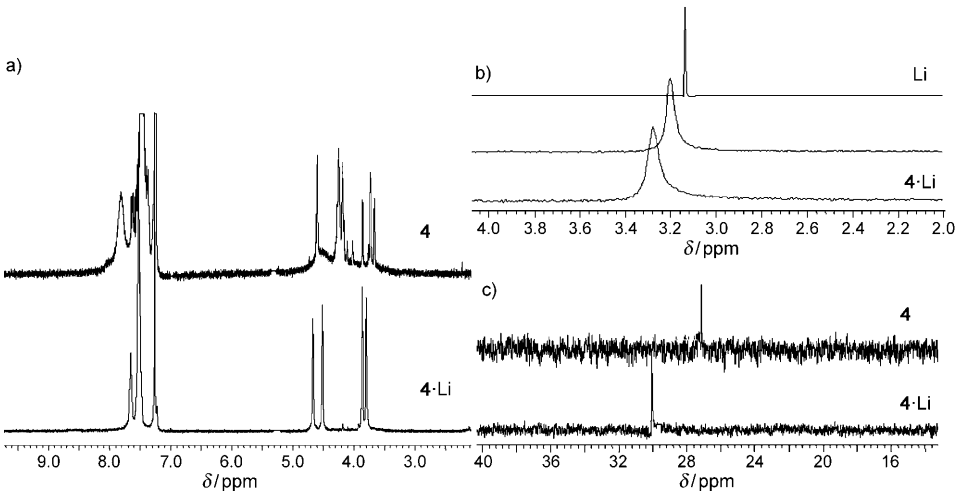

Figure 8. Changes upon complexation of receptor **4** by Li^+ cations registered in a) ^{1}H, b) ^{7}Li (0, 0.5, and 1 equiv of **4**), and c) ^{31}P NMR spectroscopy.

tion (Figure 8c). When the ^{31}P NMR spectrum of the preformed complex **4**·Li was recorded at −62 °C, two peaks at $\delta = 22.9$ and 31.7 ppm were observed. The ^{31}P NMR signal for aminophosphonium salts is generally 30–45 ppm, whereas the signal for the corresponding iminophosphoranes is generally shifted upfield and lies in the range 0–20 ppm. The appearance of two different peaks in the spectrum is clear evidence of the presence of two chemically nonequivalent phosphorus atoms, one of them with an aminophosphonium-like character and the other with a configuration resembling more a iminophosphorane group. In addition, the shift experienced by the *ipso*-carbon atom of the aromatic rings is in excellent agreement with those found in the conversion of an iminophosphorane unit into the corresponding aminophosphonium salt.[21] These spectroscopic results confirm that the complexation of the Li^+ cations by the receptor **4** gives rise to an increase in the rate of the conformational equilibrium, as is shown by the simultaneous increase in the resolution of the spectra upon addition of Li^+. A shifting of the peaks was observed in all the NMR experiments, which indicates a fast equilibrium between complexed and uncomplexed species compared with the acquisition times of these techniques. The strong interaction between the ligand and the Li^+ cation, which is shown by the high value of the association constant, is also demonstrated by the fact that the addition of a Li^+ scavenger, like 12-crown-4, to a solution containing the complex does not promote decomplexation of the cation even after stirring for 24 h. This was proven by ^1H NMR experiments that showed that after this time the signals of the complex remain unaltered (see the Supporting Information).

The coordination mode of the lithium in the complex was studied in the solid state by ^7Li, ^1H, and ^{13}C MAS NMR spectroscopy. In all cases important differences were found between the lithium salt $(C_6H_5)_4B^-Li^+$ in the presence and absence of the receptor **4**. Thus, the ^7Li NMR spectrum of the $(C_6H_5)_4B^-Li^+$ salt exhibits a signal composed of three partially superimposed peaks at $\delta = -1.24$, -1.67, and -2.54 ppm that changes to a single broad peak centered at $\delta = 0.59$ ppm upon complexation (Figure 9b). The solid-state ^{31}P NMR spectrum of the complex also shows two peaks at $\delta = 36.2$ and 17.7 ppm (Figure 9a). These results are in agreement with those found when the spectrum was recorded in solution at a low temperature. In general, all the spectral changes observed upon complexation suggest a nonsymmetrical environment of the cation inside the ligand with two different N–P bridges that interconvert rapidly when the complex is in solution, but at a lower rate in the solid state, a result that is supported by ^{31}P MAS NMR experiments. To corroborate this hypothesis, a temperature-variable ^{31}P MAS NMR experiment was performed (see the Supporting Information). A progressive approach of the two peaks is observed in the spectra with increasing temperature accompanied by a decrease in the intensity, which suggests a slight coalescence. Unfortunately, above 140 °C, the complex irreversibly decomposes without coalescence to a single peak.

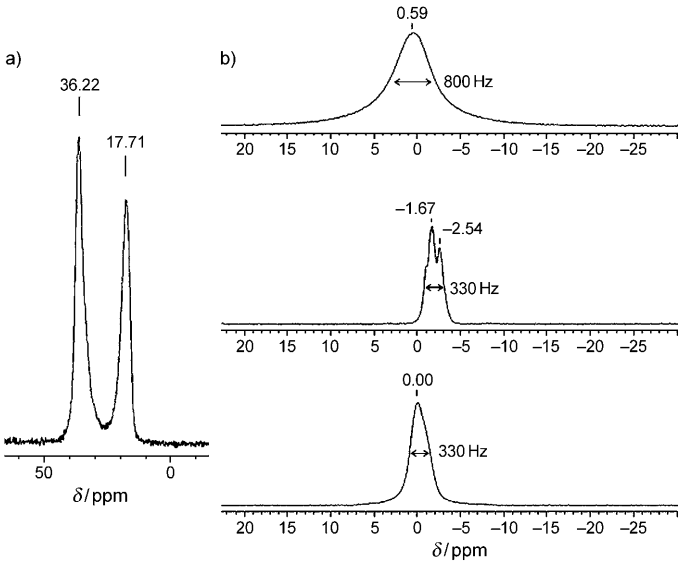

Figure 9. a) ^{31}P MAS NMR spectrum of the complex **4**·Li^+. b) ^7Li MAS NMR spectra of the complex **4**·Li^+ (top), lithium tetraphenylborate (middle), and the external reference (LiCl) (bottom).

The nature of the complex $[\mathbf{4}\cdot Li^+](C_6H_5)_4B^-$ was also confirmed by X-ray diffraction analysis. X-ray quality crystals of $[\mathbf{4}\cdot Li^+](C_6H_5)_4B^-$ were grown by slow diffusion of diisopropyl ether into a solution of $[\mathbf{4}\cdot Li^+](C_6H_5)_4B^-$ in dichloromethane. The structure of the complex in the solid state (Figure 10) belongs to the monoclinic crystal system and the *Cc* (no. 9) space group with four molecules in the unit cell.

The structure contains a [2.2]ferrocenophane ring in a highly symmetric blocked geometry, which accounts for the very well-defined NMR spectra observed for the complexed compound. Ligand **4** presents two axial and two equatorial phenyl groups with almost linear and orthogonal angles of 152 and 98°, respectively (Table 1). The two equatorial *P*-phenyl substituents present a *trans* conformation, each one pointing to a different side of the ring. The molecule presents two orientations that can be overlayed by the formal rotation of 180° of the molecule leading to complete overlaying of the ferrocene units and phenyl rings but not of the nitrogen and phosphorus bridge atoms. The ligand presents a relatively large Fe···Fe distance ($d_{Fe\cdots Fe} = 6.277$ Å) and a short distance between the bridges ($d_{N\cdots N} = 2.853$ Å, $d_{P\cdots P} = 4.705$ Å) with almost parallel ferrocenes with small dihedral angles of 1.4 and 2.3°. Each nitrogen atom forms two hydrogen bonds with a Cp–H atom and an *ortho*-hydrogen atom of the equatorial phenyl group ($d_{N\cdots CpH} = 2.675$ and 2.754 Å and $d_{N\cdots PhH} = 2.505$ and 2.760 Å). In the crystal structure, a small electron density is found on the nitrogen atom of one of the bridges. The value of this density is not large enough to be assigned to a lithium cation. This fact, together with the disorder found for the bridge over several positions and the analyses carried out confirming the presence of the lithium cation help us to postulate the presence of the Li^+ in the inner cavity of the ferrocenophane. Moreover, taking into account the disorder of the structure, the spectroscopic

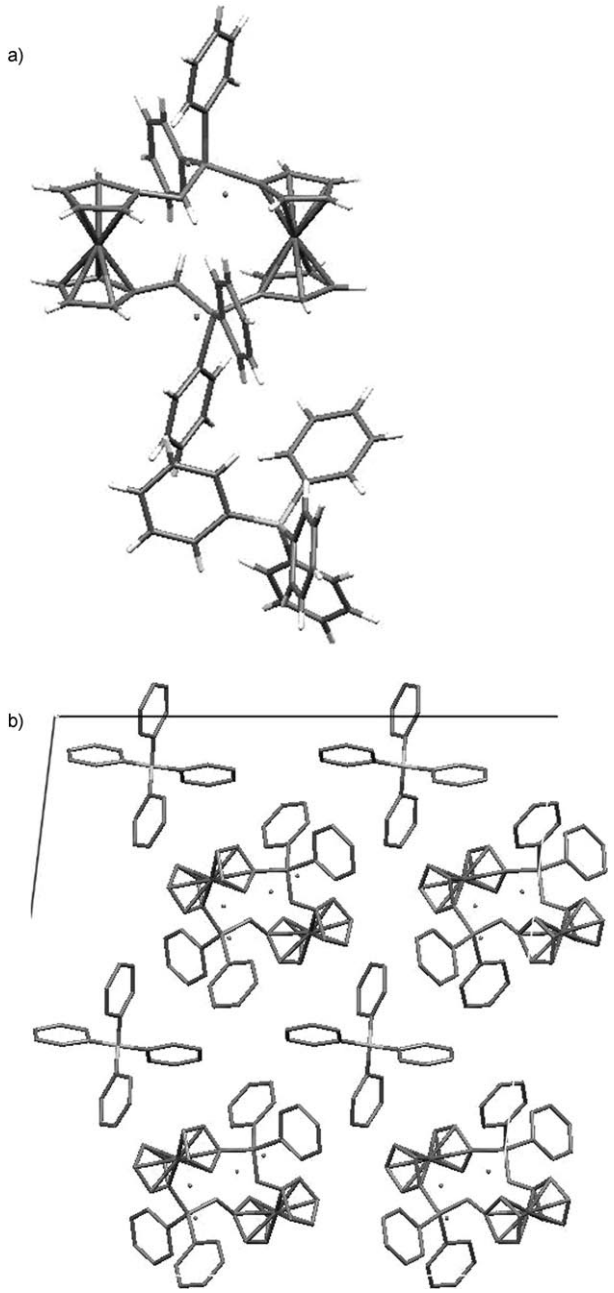

Figure 10. a) X-Ray diffraction structure of complex $[\mathbf{4}\cdot Li]^{+}(C_6H_5)_4B^{-}$. The cation Li^{+} is delocalized inside the cage between different positions. b) Crystal packing along the *b* axis.

analyses, and the positions of the atoms with binding affinity towards Li^{+}, the two nitrogen atoms and the iron, we can confirm that the Li^{+} cation must move between different positions in the cavity. In fact, it has been found that the N···N distance ($d_{N\cdots N}=2.853$ Å) is very short, which is indicative of a tweezer-like action of the two nitrogen atoms, which locates the Li^{+} cation at a very short distance from the Fe1 atom, thus fixing the conformation of the complex (Figure 10a) and confirming the postulated planetary orbit around the ferrocene.

The two pairs of phenyl units of the tetraphenylborate counterion each sandwich a ferrocene unit of two different ferrocenophane molecules with short $d_{FcpH\cdots CHPh}$ distances (< 3 Å) and also short distances (< 3 Å) to the equatorial and axial phenyl rings of two different ferrocenophanes, respectively, these interactions being the driving force for molecular packing leading to efficient space filling (Figure 10b).

To further elucidate the exact position of Li^{+} in the bridge cavity, DFT calculations were performed on the free ligand **4** as well as on the complex $[\mathbf{4}\cdot Li^{+}](C_6H_5)_4B^{-}$ and the results are summarized in Table 1.

Despite the large unfavorable contribution of desolvation of a naked lithium cation, according to our calculations the formation of the $\mathbf{4}\cdot Li^{+}$ complex is an exergonic process ($\Delta E_{CH_2Cl_2}=-1.96$ kcal mol^{-1}) that anchors the ligand in a C_2-symmetric topology (Figure 11) very much resembling that

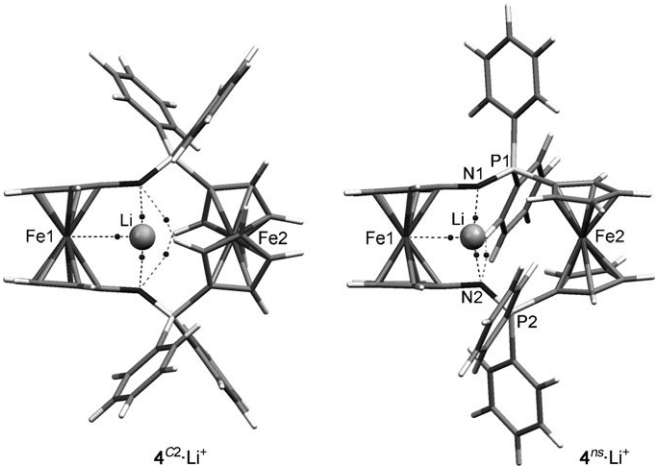

Figure 11. Calculated $\mathbf{4}^{C2}\cdot Li^{+}$ and $\mathbf{4}^{ns}\cdot Li^{+}$ complexes. Small dark spheres represent BCPs, the corresponding bond paths being sketched by dashed lines.

of the second minimum of the free ligand $\mathbf{4}^{C2b}$ (Table 1 and Figure 3) from which complexation would require little reorganization (calculated $L_{strain}=10.24$ kcal mol^{-1}). The highly symmetric blocked geometry displayed by the complex $\mathbf{4}^{C2}\cdot Li^{+}$ accounts for the very well-defined NMR spectra observed. In the complex, the Li^{+} cation lies symmetrically in the inner cavity of the host at typical bonding distances to both the iminophosphorane nitrogen atoms ($d_{N-Li}=1.895$ Å; $WBI_{N-Li}=0.040$). We also used Bader's AIM (atoms-in-molecules) methodology[22] to perform a topological analysis of the electronic charge density $\rho(r)$ to search for significant bond critical points (BCPs) around the spatial region in which cation-binding or any other type of interaction takes place. According to this theory, when two neighboring atoms are chemically bonded, a BCP appears between them. The sign of the Laplacian of the electron density at a bond critical point ($\nabla^2\rho(r_c)$) reveals whether the charge is concentrated, as in covalent bonds ($\nabla^2\rho(r_c)<0$), or depleted, as in closed-shell (electrostatic) interactions ($\nabla^2\rho(r_c)>$

0).[23] For this complex, both parameters indicate a relatively strong N–Li bond ($\rho(r_c)=3.78\times10^{-2}\,e\,a_0^{-3}$; $\nabla^2\rho(r_c)=24.84\times10^{-2}\,e\,a_0^{-5}$). However, more interesting is the fact that the tweezer-like action of the two nitrogen atoms locates the Li^+ cation within contact distance of Fe1 ($d_{Fe1-Li}=2.610$ Å; $WBI_{Fe1-Li}=0.013$), the significant binding interaction being demonstrated by the location of the corresponding BCP connecting the two atoms ($\rho(r_c)=1.61\times10^{-2}\,e\,a_0^{-3}$; $\nabla^2\rho(r_c)=5.62\times10^{-2}\,e\,a_0^{-5}$).

It is important to highlight the fact that the Li^+ cation remains essentially *N,N,Fe1*-tricoordinated in as much as we have not found any BCP that corresponds to a hypothetical interaction with the Fe2 atom despite their still relatively close proximity ($d_{Fe2\cdots Li}=3.126$ Å). Additional hydrogen-bonding between the nitrogen atoms and the cyclopentadienyl hydrogen atoms ($d_{N\cdots H}=2.867$ Å; $WBI_{N\cdots H}=0.003$; $\rho(r_c)=0.80\times10^{-2}\,e\,a_0^{-3}$; $\nabla^2\rho(r_c)=2.01\times10^{-2}\,e\,a_0^{-5}$) contribute to the fixing of the geometry (Figure 11).

Note that the single-crystal X-ray diffraction structure reported herein (Figure 10) exhibits clearly distinguished axial and equatorial *P*-phenyl groups and, consequently, it does not fit with the above-mentioned C_2-symmetric calculated geometry (Table 1). However, we have found a second non-symmetric local minimum for $\mathbf{4}^{ns}\cdot Li^+$ (Figure 11), only 1.36 kcal mol^{-1} above the former one, that shows the required axial/equatorial pattern of P-substituents with the Li^+ cation laterally displaced from the Fe1–Fe2 axis (angle Fe2···Fe1–Li 18.0°) and displays general geometric parameters that roughly agree with the experimentally obtained structure (Table 1). According to this "solid-state" calculated structure of $\mathbf{4}^{ns}\cdot Li^+$, the Li^+ cation is preferentially bonded to one nitrogen atom ($d_{N-Li}=1.888$ and 1.934 Å; $WBI_{N-Li}=0.039$ and 0.028; $\rho(r_c)=3.76\times10^{-2}$ and $3.45\times10^{-2}\,e\,a_0^{-3}$; $\nabla^2\rho(r_c)=25.33\times10^{-2}$ and $22.40\times10^{-2}\,e\,a_0^{-5}$), which causes a slightly different environment at every adjacent phosphorus atom, as experimentally found. For the P1 atom connected to the more coordinating N1 atom a higher positive natural charge variation is computed in relation to the free ligand ($\Delta q_p^n=+0.020$ and $+0.005$ au for P1 and P2, respectively). Thus, P1 is predicted to behave like an aminophosphonium-like center and the magnetic nonequivalence entails a calculated upfield shift of its ^{31}P resonance of around 7.5 ppm in comparison with the other iminophosphorane-like P2 atom. These results reflect the same tendency observed experimentally in the solid-state ^{31}P NMR spectrum (Figure 9). The tricoordination sphere around Li^+ in the complex $\mathbf{4}^{ns}\cdot Li^+$ is completed by a stronger interaction with Fe1 than in the symmetric complex ($d_{Fe1-Li}=2.564$ Å; $WBI_{Fe1-Li}=0.015$; $\rho(r_c)=1.71\times10^{-2}\,e\,a_0^{-3}$; $\nabla^2\rho(r_c)=6.27\times10^{-2}\,e\,a_0^{-5}$) and again the overall structure is additionally fixed by complementary N···H hydrogen bonds with Cp or *ortho*-Ph hydrogen atoms[24] (not shown).

Conclusions

The two prepared multinuclear [2.2]ferrocenophanes **3** and **4**, with their rather rigid and well-defined architectures, exhibit high selectivities towards metallic cations and are thus potential molecular chemosensors. In the case of receptor **3** a high selectivity towards Zn^{2+} among the cations studied was found. The recognition process was studied by electrochemical, optical, and NMR methods. The cyclic bis-iminophosphorane **4** displays an exceptionally strong binding affinity towards Li^+ compared with other alkaline cations. Only the electrochemical oxidation of the iron centers promote the decomplexation of the stable $\mathbf{4}\cdot Li^+$. A detailed study of the complex $\mathbf{4}\cdot Li^+$ by NMR (^1H, ^{13}C, ^7Li, and ^{31}P) spectroscopy in both the solid state and in solution, as well as an X-ray analysis and theoretical calculations, suggests that an additional Li···Fe interaction could explain the observed stability of the complex formed, confirming the planetary model of the Li^+ coordinated by the iron atom of the ferrocene.

Experimental Section

All reactions were carried out using solvents that were dried by routine procedures. All melting points were determined on a Kofler hot-plate melting-point apparatus and are uncorrected. IR spectra were recorded as Nujol emulsions or films on a Nicolet Impact 400 spectrophotometer. UV/Vis/Near IR spectra were recorded on a Varian Cary 5000 spectrophotometer. ^1H, ^{13}C, ^7Li, and ^{31}P NMR solution spectra were recorded on a Bruker 200, 300, 400 or 600 MHz spectrometer. ^7Li, ^{31}P, and ^{13}C solid-state MAS NMR spectra were recorded on a Bruker AV400WB spectrometer equipped with a CPMAS module. The following abbreviations for multiplicity of the signals have been used: s (singlet), m (multiplet), and q (quaternary carbon atom). Chemical shifts refer to signals measured relative to tetramethylsilane (TMS) in the case of ^1H and ^{13}C NMR spectra. The mass spectra were recorded on a Fisons AUTOSPEC 500 VG spectrometer and the FAB^+ mass spectra were recorded using 3-nitrobenzyl alcohol as the matrix. Microanalyses were performed on a Carlo–Erba 1108 instrument. Crystallographic measurements were made at 233(2) K on a Nonius KappaCCD4-circle diffractometer equipped with graphite-monochromatized $Mo_{K\alpha}$ radiation and the structure was solved by direct methods (SHELXS-97) and refinded by full-matrix least-squares methods on F^2 (SHELXL-97). The cyclic voltammetric measurements were performed on a QUICELTRON potentiostat/galvanostat controlled by a personal computer and driven by dedicated software. Cyclic voltammetry was performed with a conventional three-electrode configuration consisting of platinum working and auxiliary electrodes and a SCE reference electrode. The experiments were carried out with a 10^{-3} M solution of sample in the appropriate solvent containing 0.1 M $[(n\text{Bu})_4\text{N}]PF_6$ as the supporting electrolyte. Deoxygenation of the solutions was achieved by bubbling nitrogen for at least 10 min and the working electrode was cleaned after each run. The cyclic voltammograms were recorded with a scan rate increasing from 0.05 to 1.00 V s^{-1}. The DPV voltammograms were recorded in a suitable solvent: $\Delta E_s=4$ mV, $\Delta E_p=25$ mV, and $f=15$ Hz. Ferrocene was used as an internal reference both for potential calibration and for reversibility criteria in all the solvents used.

Calculated geometries were fully optimized in the gas phase with tight convergence criteria at the DFT level with the Gaussian 03 package[25] by using Truhlar's hybrid meta functional mPW1B95,[26] which has been recommended for general purpose applications and was developed to produce a better performance for cases in which weak interactions are involved. The 6-311G** basis set was used for all atoms, adding diffuse

functions to donor atoms (oxygen, nitrogen, and iron) (denoted as aug6-311G**). Ultrafine grids (99 radial shells and 590 angular points per shell) were employed for numerical integrations. From these gas-phase optimized geometries all reported data were obtained by single-point (SP) calculations. Energy values were computed at the same level and considering effects by using the Cossi and Barone's CPCM (conductor-like polarizable continuum model) modification[27] of Tomasi's PCM formalism.[28] Only those energies computed for the study of the atropoisomeric equilibrium of **3** and $\mathbf{3}^+$ are corrected for the zero-point vibrational energy. The same level of theory was used to perform the natural bond orbital (NBO) population analysis from which natural charges and AO energies were obtained. Bond orders were characterized by Wiberg's bond index (WBI)[29] and calculated by the NBO method as the sum of the squares of the off-diagonal density matrix elements between atoms. TD-DFT calculations were performed at the current level of theory on gas-phase optimized geometries. The B3LYP functional[30] was used in the single-point calculations. Values from the magnetic shielding tensor were obtained by using the nonrelativistic gauge-including atomic orbital (GIAO)[31] approach. The topological analysis of the electronic charge density was conducted by Bader's AIM (atoms-in-molecules)[22] methodology using the AIM2000 software.[32]

Preparation of bis(methylideneamino)[2.2](1,1″:1′,1‴)ferrocenophane (3): A solution of 1,1′-bis(triphenilphosphoranylideneamino)ferrocene (**2**; 0.40 g, 0.54 mmol) in anhydrous toluene (100 mL) was added to a solution of 1,1′-diformylferrocene (0.12 g, 0.54 mmol) in anhydrous toluene (130 mL) at room temperature and under nitrogen. The solution was heated at reflux and stirred overnight and then the solvent removed under vacuum to give a residue that was purified by chromatography on a silica gel column using CH_2Cl_2/CH_3OH (9:1) as eluent to give **3** (R_f = 0.8) in a yield of 72%, which was further recrystallized from CH_2Cl_2/Et_2O (2:1). M.p. 237–240°C (decomp.); ^{1}H NMR (200 MHz, $CDCl_3$, 25°C, TMS): δ = 4.07 (s, 4H; Fc), 4.24 (s, 4H; Fc), 5.12 (s, 4H; Fc), 5.44 (s, 4H; Fc), 9.39 ppm (s, 2H; CH=N); ^{13}C NMR (100.4 MHz, $CDCl_3$, 25°C, TMS): δ = 64.6 (CH; Cp), 67.1 (CH; Cp), 69.7 (CH; Cp), 70.4 (CH; Cp), 80.8 (q; Cp), 102.2 (q; Cp), 165.6 ppm (CH=N); IR (Nujol): $\tilde{\nu}$ = 1612 (C=N), 1035, 937, 822, 732 cm^{-1}; MS (70 eV): *m*/*z* (%): 422 (100) $[M]^+$, 357 (15), 343 (13), 211 (18); elemental analysis calcd (%) for $C_{22}H_{18}Fe_2N_2$: C 62.56, H 4.27, N 6.64; found: C 62.70, H 4.31, N 6.65.

Preparation of bis(diphenylphosphoranylideneamino)[2.2](1,1″:1′,1‴)]-ferrocenophane (4): A solution of 1,1′-bis(diphenylphosphino)ferrocene (0.207 g, 0.377 mmol) in anhydrous CH_2Cl_2 (40 mL) was added dropwise to a solution of 1,1′-diazidoferrocene (0.10 g, 0.37 mmol) in anhydrous CH_2Cl_2 (40 mL) at room temperature and under nitrogen. The mixture was stirred for 4 h and then three quarters of the volume was removed under vacuum. Dimethyl ether/*n*-hexane (2:1; 40 mL) was added to the mixture and the precipitate formed was recrystallized in anhydrous CH_2Cl_2/Et_2O (1:1) to give the product in a yield of 73%. M.p. 181–185°C (decomp.); ^{1}H NMR (400 MHz, $CDCl_3$, 25°C, TMS): δ = 3.62 (s, 1H; Fc), 3.68 (s, 2H; Fc), 3.82 (s, 1H; Fc), 4.15 (s, 2H; Fc), 4.27–4.16 (m, 6H; Fc), 4.63 (s, 4H; Fc), 7.47–7.56 ppm (m, 20H; Ar); ^{13}C NMR (100.4 MHz, $CDCl_3$, 25°C, TMS): δ = 63.3 (CH; Cp), 64.2 (CH; Cp), 73.3 (d, ^2J(C,P) = 12.0 Hz, CH; Cp), 73.4 (d, ^2J(C,P) = 12.0 Hz, CH; Cp), 73.9 (d, ^3J(C,P) = 10.5 Hz, CH; Cp), 74.1 (d, ^1J(C,P) = 114.1 Hz, q; Cp), 74.4 (d, ^3J(C,P) = 10.5 Hz, CH; Cp), 128.2 (d, ^2J(C,P) = 122.2 Hz, CH; Ar), 128.3 (d, ^2J-(C,P) = 12.2 Hz, CH; Ar), 131.2 (d, ^3J(C,P) = 9.6 Hz, CH; Ar), 131.6 (CH; Ar), 132.1 (d, ^3J(C,P) = 9.6 Hz, CH; Ar), 133.8 ppm (d, ^1J(C,P) = 106.4 Hz, q; Ar); IR (Nujol): $\tilde{\nu}$ = 1457, 1437, 1289, 1171, 1112, 1080, 829, 751, 723, 701 cm^{-1}; MS (FAB$^+$): *m*/*z* (%): 767 (100) $[M+1]^+$; elemental analysis calcd (%) for $C_{44}H_{36}Fe_2N_2P_2$: C 68.95, H 4.73, N 3.66; found: C 68.69, H 4.91, N 3.49.

X-ray data for the complex $[\mathbf{4}\cdot Li^+](C_6H_5)_4B^-$: $C_{68}H_{57}BFe_2N_2P_2$, T = 233(2) K, λ = 0.71073 Å, monoclinic, space group *Cc* (no. 9), a = 26.5447(2), b = 8.4424(3), c = 23.6205(7) Å, α = 90, β = 96.873(2), γ = 90°, volume = 5255.3(2) Å^3, ρ_{calcd} = 1.373 Mg m^{-3}, F(000) = 2264, crystal size 0.4 × 0.15 × 0.06 mm^3, 12311 reflections collected, 7383 independent reflections R(int) = 0.0252, goodness-of-fit on F^2 = 1.056, R indices (all data) $R1$ = 0.0460, $wR2$ = 0.0862.

CCDC-731094 (**4**) contains the supplementary crystallographic data for this paper. These data can be obtained free of charge from The Cambridge Crystallographic Data Centre via www.ccdc.cam.ac.uk/data_request/cif.

Acknowledgements

We gratefully acknowledge the financial support from MICINN-Spain (Projects CTQ2008-01402 and "Eje C-Consolider" EMOCIONa CTQ2006-06333/BQU), from the Fundación Séneca (Agencia de Ciencia y Tecnología de la Región de Murcia; Programa de Ayudas a Grupos de Excelencia de la Región de Murcia, Plan Regional de Ciencia y Tecnología 2007/2010, project 04509/GERM/06), from the Generalitat de Catalunya (grant no. SGR-00591), and from the CIBER de Bioingeniería, Biomateriales y Nanomedicina (CIBER-BBN, promoted by ISCIII) of Spain.

[1] a) T. Wright, E. V. Anslyn, *Chem. Soc. Rev.* **2006**, *35*, 14–28; b) P. A. Gale, *Acc. Chem. Res.* **2006**, *39*, 465–475; c) A. P. de Silva, B. McCaughan, B. O. F. McKinney, M. Querol, *Dalton Trans.* **2003**, 1902–1913; d) S. L. Wiskur, H. Ait-Haddou, J. J. Lavigne, E. V. Anslyn, *Acc. Chem. Res.* **2001**, *34*, 963–972; e) T. Gunnlaugsson, J. P. Leonard, *Chem. Commun.* **2005**, 3114–3131; f) T. Gunnlaugsson, P. E. Kruger, P. Jensen, J. Tierney, H. D. P. Ali, G. M. Hussey, *J. Org. Chem.* **2005**, *70*, 10875–10878; g) T. Gunnlaugsson, H. D. P. Ali, M. Glynn, P. E. Kruger, G. M. Hussey, F. M. Pfeffer, C. M. G. dos Santos, J. Tierney, *J. Fluoresc.* **2005**, *15*, 287–299.

[2] a) P. D. Beer, *Chem. Soc. Rev.* **1989**, *18*, 409–450; b) P. D. Beer, P. A. Gale, G. Z. Chen, *Coord. Chem. Rev.* **1999**, *185–186*, 3- 36; c) P. D. Beer, P. A. Gale, G. Z. Chen, *J. Chem. Soc. Dalton Trans.* **1999**, 1897–1909; d) P. D. Beer, D. K. Smith, *J. Chem. Soc. Dalton Trans.* **1998**, 417–423; e) J. D. Carr, S. J. Coles, W. W. Hassan, M. B. Hursthouse, K. M. A. Malik, J. H. R. Tucker, *J. Chem. Soc. Dalton Trans.* **1999**, 57–62; f) S. Barlow, H. E. Bunting, C. Ringham, J. C. Green, G. U. Bublitz, S. G. Boxer, J. W. Perry, S. R. Marder, *J. Am. Chem. Soc.* **1999**, *121*, 3715–3723; g) S. Fery-Forgues, B. Delavaux-Nicot, *J. Photochem. Photobiol. A* **2000**, *132*, 137–159; h) P. D. Beer, A. R. Graydon, L. R. Sutton, *Polyhedron* **1996**, *15*, 2457–2461; i) F. Sancenón, A. Benito, F. J. Hernández, J. M. Lloris, R. Martínez-Máñez, T. Pardo, J. Soto, *Eur. J. Inorg. Chem.* **2002**, 866–875; j) B. Delavaux-Nicot, J. Maynadié, D. Lavabre, S. Fery-Forgues, *Inorg. Chem.* **2006**, *45*, 5691–5702; k) P. Molina, A. Tárraga, A. Caballero, *Eur. J. Inorg. Chem.* **2008**, 3401–3417.

[3] For a review, see: R. W. Heo, T. R. Lee, *J. Organomet. Chem.* **1999**, *578*, 31–42.

[4] a) A. Caballero, V. Lloveras, A. Tárraga, A. Espinosa, M. D. Velasco, J. Vidal-Gancedo, C. Rovira, K. Wurst, P. Molina, J. Veciana, *Angew. Chem.* **2005**, *117*, 2013–2017; *Angew. Chem. Int. Ed.* **2005**, *44*, 1977–1981; b) F. Otón, A. Tárraga, P. Molina, *Org. Lett.* **2006**, *8*, 2107–2110; c) F. Otón, A Espinosa, A. Tárraga, C. Ramírez de Arellano, P. Molina, *Chem. Eur. J.* **2007**, *13*, 5742–5752.

[5] a) D. Seyferth, B. W. Hames, T. G. Rucker, M. Cowle, R. S. Dickson, *Organometallics* **1983**, *2*, 472–474; b) S. Akabori, T. Yumagai, T. Shirahige, S. Sato, K. Kawazoe, C. Tamura, M. Sato, *Organometallics* **1987**, *6*, 2105–2109; c) J. C. Medina, T. T. Goodnow, M. T. Rojas, J. L. Atwood, B. C. Lynn, A. E. Kaifer, G. W. Gokel, *J. Am. Chem. Soc.* **1992**, *114*, 10583–10595.

[6] a) P. Burk, I. A. Koppel, I. Koppel, R. Kur, J.-F. Gal, P.-C. Maria, M. Herreros, R. Notario, J.-L. M. Abboud, I. Anvia, R. F. Taft, *J. Phys. Chem. A* **2000**, *40*, 1424–1427; b) A. Irigoras, J. M. Mercero, I. Silanes, J. M. Ugalde, *J. Am. Chem. Soc.* **2001**, *123*, 5040–5043; c) J. Rodriguez-Otero, E. M. Cabaleiro-Lago, A. Peña-Gallego, M. M. Montero-Campillo, *Tetrahedron* **2009**, *65*, 2368–2371.

[7] M. Scheibitz, R. F. Winter, M. Bolte, H.-W. Lerner, M. Wagner, *Angew. Chem.* **2003**, *115*, 954–957; *Angew. Chem. Int. Ed.* **2003**, *42*, 924–927.
[8] a) "Zinc: Lewis Acid Catalysis and Regulation": J. J. R. F. da Silva, R. J. P. Williams in *The Biological Chemistry of Elements: The Inorganic Chemistry of Life*, 2nd ed., Oxford University Press, New York, **2001**; b) R. J. P. Williams, J. J. R. F. da Silva, *Coord. Chem. Rev.* **2000**, *200–202*, 247–348.
[9] B. L. Vallee, K. H. Falchuk, *Physiol. Rev.* **1993**, *73*, 79–118.
[10] a) E. Ho, B. N. Ames, *Proc. Natl. Acad. Sci. USA* **2002**, *99*, 16770–16775; b) H. Daiyasu, K. Osaka, Y. Ishino, H. Toh, *FEBS Lett.* **2001**, *503*, 1–6.
[11] A. Q. Truong-Tran, J. Carter, R. E. Ruffin, P. D. Zalewski, *Biometals* **2001**, *14*, 315–330.
[12] Interalia, see: a) F. Zapata, A. Caballero, A. Espinosa, A. Tárraga, P. Molina, *Org. Lett.* **2007**, *9*, 2385–2388; b) S. Sreejith, K. P. Divya, A. Ajayaghosh, *Chem. Commun.* **2008**, 2903–2905; c) Y. Mikata, A. Yamashita, A. Kawamura, H. Kouno, Y. Miyamoto, S. Tamotsu, *Dalton Trans.* **2009**, 3800–3806; d) E. N. Nolan, S. J. Lippard, *Acc. Chem. Res.* **2009**, *42*, 193–203.
[13] For a review, see: a) K. Dehnicke, M. Frieger, W. Massa, *Coord. Chem. Rev.* **1999**, *182*, 19–65. For recent references, see: b) A. Arques, D. Auñón, P. Molina, *Tetrahedron Lett.* **2004**, *45*, 4337–4340; c) R. Bielsa, R. Navarro, T. Soler, E. P. Urriolabeitia, *Dalton Trans.* **2008**, 1203–1214; d) D. Aguilar, M. A. Aragüés, R. Bielsa, E. Serrano, T. Soler, R. Navarro, E. P. Urriolabeitia, *J. Organomet. Chem.* **2008**, *693*, 417–424; e) R. Bielsa, R. Navarro, E. P. Urriolabeitia, A. Lledós, *Inorg. Chem.* **2007**, *46*, 10133–10142; f) D. Aguilar, M. Contel, R. Navarro, E. P. Urriolabeitia, *Organometallics* **2007**, *26*, 4604–4611; g) S. D. J. Brown, W. Henderson, K. J. Kilpin, B. K. Nicholson, *Inorg. Chim. Acta* **2007**, *360*, 1310–1315; h) L. J. L. Häller, N. Kaltsoyannis, M. J. Sarsfield, I. May, S. M. Cornet, M. P. Redmond, M. Helliwell, *Inorg. Chem.* **2007**, *46*, 4868–4875; i) P. Oulié, C. Freund, N. Saffon, B. Martín-Vaca, L. Maron D. Bourisson, *Organometallics* **2007**, *26*, 6793–6804.
[14] A. Tárraga, F. Otón, A. Espinosa, M. D. Velasco, P. Molina, D. J. Evans, *Chem. Commun.* **2004**, 458–459.
[15] a) P. Molina, M. J. Vilaplana, *Synthesis* **1994**, 1197–1218; b) A. Arques, P. Molina, *Curr. Org. Chem.* **2004**, *8*, 827–843.
[16] The DPV technique was employed to obtain well-resolved potential information whereas the individual redox processes are poorly resolved in the CV experiments as individual $E_{1/2}$ potentials cannot be accurately extracted easily from this data. See: B. Serr, K. A. Andersen, C. M. Elliot, O. P. Anderson, *Inorg. Chem.* **1988**, *27*, 4499–4504.
[17] a) C. D. Hall, G. J. Kirkovits, A. C. Hall, *Chem. Commun.* **1999**, 1897–1898; b) A. Caballero, A. Espinosa, A. Tárraga, P. Molina, *J. Org. Chem.* **2008**, *73*, 5489–5497; c) A. Caballero, V. Lloveras, D. Curiel, A. Tárraga, A. Espinosa, R. García, J. Vidal-Gancedo, C. Rovira, K. Wurst, P. Molina, J. Veciana, *Inorg. Chem.* **2007**, *46*, 825–838.
[18] a) S. R. Marder, J. W. Perry, B. G. Tiemann, *Organometallics* **1991**, *10*, 1896–1901; b) B. J. Coe, C. J. Jones, J. A. McCleverty, D. Bloor, G. J. Cross, *J. Organomet. Chem.* **1994**, *464*, 225–232; c) T. J. Müller, A. Netz, M. Ansorge, *Organometallics* **1999**, *18*, 5066–5074; d) J. D. Carr, S. J. Coles, M. B. Hassan, M. B. Hurthouse, K. M. A. Malik, J. H. R. Tucker, *J. Chem. Soc. Dalton Trans.* **1999**, 57–62.
[19] Specfit/32 Global Analysis System, 1999–2004 Spectrum Software Associates (SpecSoft@compuserve.com). The Specfit program was acquired from Bio-logic S.A. (http://www.bio-logic.info) in January 2005. The equation to be adjusted by non-linear regression using the above-mentioned software was: $\Delta A/b = (K_{11}\Delta\varepsilon_{HG}[H]_{tot}[G])/(1+K_{11}[G])$, where H = host, G = guest, HG = complex, ΔA = variation in the absorption, b = cell width, K_{11} = association constant for a 1:1 model and $\Delta\varepsilon_{HG}$ = variation of molar absorptivity.
[20] M. Shortreed, R. Kopelman, M. Kuhn, B. Hoyland, *Anal. Chem.* **1996**, *68*, 1414–1418.
[21] a) J. Laynez, M. Menendez, J. L. Saiz Velasco, A. L. Llamas-Saiz, C. Foces-Foces, J. Elguero, P. Molina, M. Alajarin, A. Vidal, *J. Chem. Soc. Perkin Trans. 1* **1993**, 709–713; b) A. L. Llamas-Saiz, C. Foces-Foces, J. Elguero, I. Aguilar-Parrilla, H.-H. Limbach, P. Molina, M. Alajarin, A. Vidal, R. M. Claramunt, C. López, *J. Chem. Soc. Perkin Trans. 2* **1994**, 209–212.
[22] R. F. W. Bader, *Atoms in Molecules: A Quantum Theory*, Oxford University Press, Oxford, **1990**.
[23] a) W. Nakanishi, T. Nakamoto, S. Hayashi, T. Sasamori, N. Tokitoh, *Chem. Eur. J.* **2007**, *13*, 255–268; b) L. Zhang, F. Ying, W. Zu, P. C. Hiberty, S. Shaik, *Chem. Eur. J.* **2009**, *15*, 2979–2989.
[24] N2···HPh interaction: $d_{N\cdots H}$ = 2.565 Å; $WBI_{N\cdots H}$ = 0.006; $\rho(r_c) = 0.93\times10^{-2}$ e a_0^{-3}; $\nabla^2\rho(r_c) = 2.59\times10^{-2}$ e a_0^{-5}. N1···HCp interaction: $d_{N\cdots H}$ = 2.743 Å; $WBI_{N\cdots H}$ = 0.001; no BCP was found.
[25] Gaussian 03, Revision B.03, M. J. Frisch, G. W. Trucks, H. B. Schlegel, G. E. Scuseria, M. A. Robb, J. R. Cheeseman, J. A. Montgomery, Jr., T. Vreven, K. N. Kudin, J. C. Burant, J. M. Millam, S. S. Iyengar, J. Tomasi, V. Barone, B. Mennucci, M. Cossi, G. Scalmani, N. Rega, G. A. Petersson, H. Nakatsuji, M. Hada, M. Ehara, K. Toyota, R. Fukuda, J. Hasegawa, M. Ishida, T. Nakajima, Y. Honda, O. Kitao, H. Nakai, M. Klene, X. Li, J. E. Knox, H. P. Hratchian, J. B. Cross, V. Bakken, C. Adamo, J. Jaramillo, R. Gomperts, R. E. Stratmann, O. Yazyev, A. J. Austin, R. Cammi, C. Pomelli, J. W. Ochterski, P. Y. Ayala, K. Morokuma, G. A. Voth, P. Salvador, J. J. Dannenberg, V. G. Zakrzewski, S. Dapprich, A. D. Daniels, M. C. Strain, O. Farkas, D. K. Malick, A. D. Rabuck, K. Raghavachari, J. B. Foresman, J. V. Ortiz, Q. Cui, A. G. Baboul, S. Clifford, J. Cioslowski, B. B. Stefanov, G. Liu, A. Liashenko, P. Piskorz, I. Komaromi, R. L. Martin, D. J. Fox, T. Keith, M. A. Al-Laham, C. Y. Peng, A. Nanayakkara, M. Challacombe, P. M. W. Gill, B. Johnson, W. Chen, M. W. Wong, C. Gonzalez, J. A. Pople, Gaussian Inc., Wallingford CT, **2004**.
[26] a) Y. Zhao, D. G. Truhlar, *J. Phys. Chem. A* **2004**, *108*, 6908–6918; b) Y. Zhao, D. G. Truhlar, *J. Phys. Chem. A* **2005**, *109*, 5656–5667.
[27] a) V. Barone, M. Cossi, *J. Phys. Chem. A* **1998**, *102*, 1995–2001; b) M. Cossi, N. Rega, G. Scalmani, V. Barone, *J. Comput. Chem.* **2003**, *24*, 669–681.
[28] a) S. Miertus, E. Scrocco, J. Tomasi, *J. Chem. Phys.* **1981**, *74–75*, 117–129; b) R. Cammi, B. Mennucci, J. Tomasi, *J. Phys. Chem. A* **2000**, *104*, 5631–5637.
[29] K. Wiberg, *Tetrahedron* **1968**, *24*, 1083–1096.
[30] L. J. Bartolotti, K. Fluchick in *Reviews in Computational Chemistry, Vol. 7*, (Eds.: K. B. Lipkowitz, D. B. Boyd), VCH, Weinheim, **1996**, pp. 187–216.
[31] J. R. Cheeseman, G. W. Trucks, T. A. Keith, M. J. Frisch, *J. Chem. Phys.* **1996**, *104*, 5497–5509.
[32] a) AIM2000 v. 2.0, designed by F. W. Biegler-König, J. Schönbohm, 2002. Homepage http://www.aim2000.de/. F. Biegler-König, J. Schönbohm, D. J. Bayles, *Comput. Chem.* **2001**, *22*, 545–559; b) F. Biegler-König, J. Schönbohm, *J. Comput. Chem.* **2002**, *23*, 1489–1494.

Received: May 27, 2009
Revised: October 16, 2009
Published online: December 9, 2009

